Accurately extracting silicon waveguide dimensions from a single high-order Mach-Zehnder Interferometer

YICHEN LIU,[1,2,*] **UMAR KHAN,**[1,2] **AND WIM BOGAERTS**[1,2]

[1] *Photonics Research Group, Ghent University-IMEC, Ghent, Belgium*
[2] *Center of Nano and Biophotonics, Ghent, Belgium*
*yichen.liu@ugent.be

Abstract: We experimentally demonstrate a new methodology for the extraction of dimensions from silicon-on-insulator (SOI) strip waveguides manufactured in IMEC's iSiPP50G silicon photonics platform. The effective index (n_{eff}) and group index (n_g) of the waveguide are determined from the spectral data of a single high-order Mach-Zehnder Interferometer (MZI). In this study, we introduce an innovative mapping model that effectively relates the geometric dimensions of the SOI waveguide to its n_{eff} and n_g, thereby enhancing mapping accuracy and reducing model complexity. Furthermore, we will elucidate the feasibility and constraints for extracting n_{eff} and n_g through the optical transmission measurement of only a single high-order MZI. Our analysis also addresses the parameter extraction errors that have a significant impact on the results, which have not been previously discussed in the literature.

1. Introduction

Over the past two decades, Silicon-on-Insulator (SOI), characterized by a high refractive index contrast, has become a commonplace material system for the fabrication of complex optical waveguide circuits [1,2]. While high refractive index contrast components can effectively minimize the overall footprint of a circuit, the effective index of refraction (n_{eff}) of waveguides and their dispersion exhibit very high sensitivity to fabrication deviations, presenting a significant challenge to achieve high production yield [3]. This is especially true for the implementation of waveguide filters based on interferometric or resonant waveguide circuits.

Dimensional deviations in waveguides, encompassing variations in width and thickness, can manifest at different levels, including variations across distinct locations on a die, across different dies on the same wafer, and across various wafers [3]. To address the issue of improving product yield, several strategies have been implemented, including the employment of tunable circuits, the design of components that exhibit lower sensitivity to fabrication deviations, and the real-time calculation of deviations at individual positions on the wafer. The last method does not directly enhance manufacturing yield; however, it enables compensation for anticipated errors during circuit design. This approach necessitates the precise estimation of variability statistics derived from fabricated wafers. This paper concentrates on the challenge of accurately extracting waveguide geometric parameters post-fabrication, utilizing a minimal number of optical measurements.

Measuring waveguide dimensions can be done by direct inspection (e.g. SEM, scatterometry) but these techniques are limited in resolution. As the optical properties of the waveguides are very sensitive to geometric variations, it makes sense to use those same waveguides for the geometry extraction. Recent years have witnessed a number of related studies exploring various waveguide components and circuits for extraction purposes. For instance, Dwivedi *et al.* implemented a method utilizing two closely situated low-order Mach-Zehnder Interferometers (MZIs) to extract n_{eff}, alongside another high-order MZI to ascertain n_g [4]. Zhang *et al.*

illustrated the extraction process using two racetrack micro-ring resonators (MRRs) with differing perimeters [5]. However, employing multiple devices introduces complications, such as increased footprint and the necessity for multiple measurements, which introduce their own variability and uncertainty. Furthermore, there is an underlying assumption that these multiple devices have identical parameters, a condition that may not accurately reflect reality. In the work of Xing *et al.*, a folded cascaded Mach-Zehnder Interferometer (C-MZI) was proposed, wherein a compact design significantly enhances the precision of extraction with fewer measurements [6]. In this methodology, the waveguide's n_g is utilized to estimate the range of n_{eff}. Nevertheless, the extraction process necessitates fitting the spectrum of the C-MZI with numerous parameters, which can lead to heightened correlations among these parameters and an long fitting time.

Similar methodologies have been employed to compute the width and thickness of the waveguide simultaneously from n_{eff} and n_g. As delineated in [7], implementing first- and second-order polynomial models can yield substantial mapping errors. Although third-order polynomial models may exhibit reduced error margins in simulations, they require a minimum of 20 coefficients.

To adress these issues, we propose a novel fast convergence iterative algorithm, designed to be used together with a single high-order MZI. Additionally, the extraction errors noted in prior research are often have a very small value ($\approx$0.1 nm), which we believe is due to several critical factors that have yet to be fully explored. This article will elucidate these factors in detail.

2. Waveguide geometry model and two steps of parameter extraction

2.1. Waveguide geometry cross-section

In Fig. 1, the cross-sectional model of the SiO_2-clad waveguide geometry utilized in our analysis is illustrated. The width of the waveguide at the base of the core is referred to as w while the thickness is represented as t. Based on our cross-section scanning electron microscopy (XSEM) images of the waveguide dimensional metrology structures, we observe that the waveguides typically exhibit an isosceles trapezoidal shape with a base angle of approximately 85°, rather than a rectangular profile.
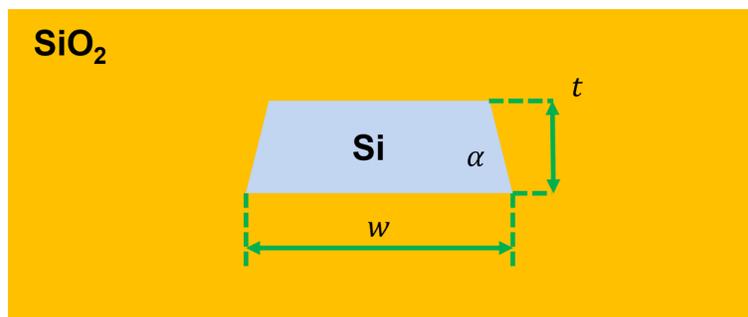
Fig. 1. SiO_2-clad waveguide geometry cross-section model.

We have conducted high-precision measurements of thickness and width on manufactured standard waveguides, specifically fully etched silicon strip waveguides designed with a width w of 450 nm within an unprocessed thickness $t = 220$ nm Silicon-On-Insulator (SOI) layer, using the IMEC iSiPP50G silicon photonics Process Design Kit (PDK). The thickness is measured utilizing an ellipsometer on an 80 µm × 80 µm uniform pad at one metrology location per die, while the waveguide linewidth is assessed automatically using a critical dimension scanning electron microscope (CD-SEM) at one metrology location per die. The results indicate that the actual average width and thickness of the standard waveguide are approximately 458 nm and 212 nm,

respectively. The maximum deviations observed for the width and thickness measurements are around 35 nm and 3 nm, respectively.

2.2. Two steps of parameter extraction

The extraction of waveguide geometric parameters comprises two distinct steps:

1. Extracting the effective index of refraction (n_{eff}) and the group index (n_g) from the measured spectrum of the circuit.

2. Subsequently extracting the width and thickness from the extracted n_{eff} and n_g.

These constitute the essential steps in the design of a circuit for parameter extraction. This article will not delve into more efficient circuit configurations at this time and will instead concentrate on employing just one single-stage MZI. The decision against utilizing a single-ring configuration is based on fact that the optical parameters of a bend and a straight waveguide segments can differ, and the uncertainties regarding the phase shift introduced by the directional coupler (DC) within the ring.

In the following section, we will outline the design of this MZI, taking into account typical fabrication deviations for waveguide dimensions and detailing the methodology for correlating geometric dimensions to waveguide indices.

3. Waveguide fabrication deviations and optical property simulation

3.1. Fabrication deviations

Based on the high-precision measurements of waveguide dimensions discussed in the preceding chapter, the maximum observed fabrication deviations in width and thickness are approximately $dw = 35$ nm and $dt = 3$ nm, respectively. To assess the impact of these deviations, we performed simulations using the finite difference eigenmode (FDE) solver in the ANSyS Lumerical MODE software. It should be noted that instead of utilizing the silicon refractive index database provided within Lumerical, we imported data sourced from Frante, available on the website refractiveindex.info.

3.2. Different silicon refractive index databases

In this section, we will present the real part of the refractive index of silicon conducted at different wavelengths. We have compared data from H.H. Li (293 K) [8] and D. Franta (293 K) [9], which can be obtained from refractiveindex.info and the database in Lumerical [10]. The results of this comparison are illustrated in Fig. 2.

The refractive index in Lumerical exhibits a discontinuity at a wavelength of 1.532 μm (Fig. 2, red points), resulting in a corresponding jump in the calculated group index at this wavelength, quantified at 0.08. This discontinuity is a numerical artifact not apparent when extracting the group index (n_g) from the measurement spectrum. Consequently, this jump in n_g introduces a variation in the extracted width of 40 nm. While this issue can be addressed by fitting the refractive index, the resulting fitted value may diverge from the original data points, and the selection of different fitting ranges will significantly influence the results.

The data provided by Franta has been selected as our mapping database due to its recency (2017), in contrast to Li's data, which originates from measurements conducted in 1980. Additionally, we will explore the differences in the extracted results when utilizing Li's databases in the error analysis section.

3.3. Waveguide n_{eff} simulation

We simulate the effective refractive index of waveguides of different widths and thicknesses at a wavelength of $\lambda = 1550$ nm and plot the results in Fig. 3. In the simulation of the waveguide's
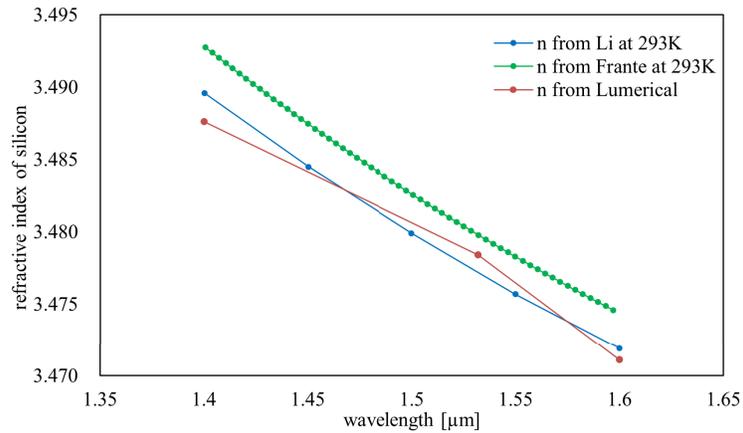
Fig. 2. Silicon refractive index from different databases.

n_{eff} and n_g, the width ranges from 400 nm to 640 nm, and the thickness ranges from 200 nm to 224 nm, with a step size of 4 nm for both parameters.
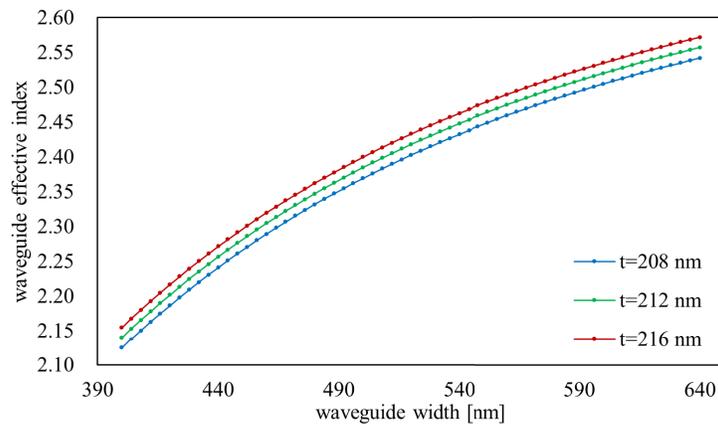
Fig. 3. Effective index of waveguide with different width and thickness.

The sensitivities of the effective index of a 'typical' waveguide ($w = 450$ nm , $t = 212$ nm) to its width and thickness are calculated as:

$$\frac{\partial n_{eff}}{\partial w}|_{\text{typical}} = 0.0024 \text{ nm}^{-1} \tag{1}$$

$$\frac{\partial n_{eff}}{\partial t}|_{\text{typical}} = 0.0037 \text{ nm}^{-1}. \tag{2}$$

It is worth mentioning that the calculated n_{eff} change is only for a 'typical' waveguide. If the waveguide shape changes significantly, it needs to be recalculated according to the waveguide shape.

Utilizing the equations presented above, one can assess the influence of fabrication deviations in waveguides on the effective index of the waveguide. During the calculation, the maximum

variations of width and thickness were set to 35 nm and 3 nm, respectively.

$$dn_{eff} = \left|\frac{\partial n_{eff}}{\partial w}dw\right| + \left|\frac{\partial n_{eff}}{\partial t}dt\right| = 0.0951 \tag{3}$$

In this context, we utilize dn_{eff} to represent the maximal deviations in n_{eff}. Although n_{eff} exhibits less sensitivity to width compared to thickness, the contribution of width deviations is $\left|\frac{\partial n_{eff}}{\partial w}dw\right| = 0.084$, which is 88 % of total dn_{eff}.

An interfering structure, such as a ring or a MZI, will exhibit a phase delay characterized by the following expression:

$$\phi = 2\pi m = \frac{2\pi n_{eff}\Delta L}{\lambda}. \tag{4}$$

The variable m denotes the interference orders, while λ represents the resonance wavelength, and ΔL signifies the physical path length difference. Should the uncertainty of n_{eff} become excessive, there exists a potential for confusion between adjacent interference orders. Consequently, it is imperative that ΔL adheres to the following principle to prevent ambiguity in the interference orders:

$$\Delta L < \frac{\lambda}{dn_{eff}}. \tag{5}$$

Based on our calculations of the effective index n_{eff}, and the 1550 nm laser source utilized for measurements, it is essential to design the length difference ΔL to be shorter than 16.30 μm. As demonstrated in Eq. (4), the phase delay in the spectrum induced by n_{eff} is proportional to ΔL. While a reduced ΔL mitigates the risk of misidentifying the order of interference, it concurrently diminishes the precision of the extracted n_{eff}.

Furthermore, there are additional complexities associated with employing short-delay-length MZIs that cannot be quantified. For instance, the phase variations described in Eq. (4) are not solely contingent upon the arm length difference; rather, they are also affected by whether the phase difference between the two DCs output ports achieves $\pi/2$. Should the two DC waveguides lack perfect symmetry, this phase difference will deviate from $\pi/2$, rendering the characterization of this factor more intricate. Therefore, we decide to design circuits with a longer delay length to enhance the phase delay contribution from n_{eff}.

3.4. Waveguide n_g calculation

We conducted a simulation of the group index for waveguides with varying widths and thicknesses, and we present the results for a wavelength of 1550 nm in Fig. 4.

The sensitivities of the group index for a 'typical' waveguide (width = 450 nm, thickness = 212 nm) have been calculated in relation to variations in its dimensions.

$$\frac{\partial n_g}{\partial w}\big|_{\text{typical}} = -0.0020 \text{ nm}^{-1} \tag{6}$$

$$\frac{\partial n_g}{\partial t}\big|_{\text{typical}} = 0.0020 \text{ nm}^{-1} \tag{7}$$

The given dimensions of the waveguide, the absolute values of the sensitivity of the refractive index to the waveguide width ($\partial n_{eff}/\partial w$) and thickness ($\partial n_{eff}/\partial t$) are comparable. This observation provides a foundation for our proposed extraction method. As shown in Eq. (8), when we estimate the uncertainty of waveguide $n_g(\Delta n_g)$, it can be calculated from the uncertainty of waveguide width(Δw) and the uncertainty of thickness(Δt):

$$\Delta n_g = \frac{\partial n_g}{\partial w} \times \Delta w + \frac{\partial n_g}{\partial t} \times \Delta t. \tag{8}$$

If n_g is extracted from the interference spectrum and the circuit used for measurement has a long delay length, then we temporarily assume that the uncertainty of n_g can be ignored. The Δw
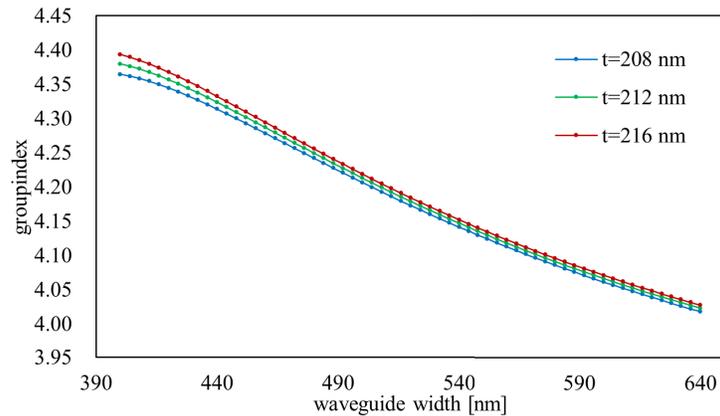
Fig. 4. Group index of waveguide with different width and thickness.

is then calculated using Eq. (9):

$$\frac{\partial n_g}{\partial w} \times \Delta w = -\frac{\partial n_g}{\partial t} \times \Delta t \Rightarrow \Delta w = -\frac{\partial n_g}{\partial t} / \frac{\partial n_g}{\partial w} \times \Delta t. \tag{9}$$

This shows that if n_g can be extracted with a high accuracy from the measured spectrum, the uncertainty in the waveguide width will no longer be determined by the maximum width manufacturing error, but by the maximum waveguide thickness manufacturing error together with the factor $\frac{\partial n_g}{\partial t} / \frac{\partial n_g}{\partial w}$. Given that the typical manufacturing error in waveguide thickness is approximately 3 nm, factor $\frac{\partial n_g}{\partial t} / \frac{\partial n_g}{\partial w}$ is generally less than or equal to 1. As a result, the uncertainty in waveguide width is reduced from the maximum manufacturing error (exceeding 30 nm) to approximately 3 nm.

3.5.   *Waveguide simulated by FEM in COMSOL Multiphysics*

We also employ COMSOL Multiphysics to simulate the n_{eff} of the waveguide. For the computation of the n_g, we selecte 11 wavelength sampling points at equal intervals within the wavelength
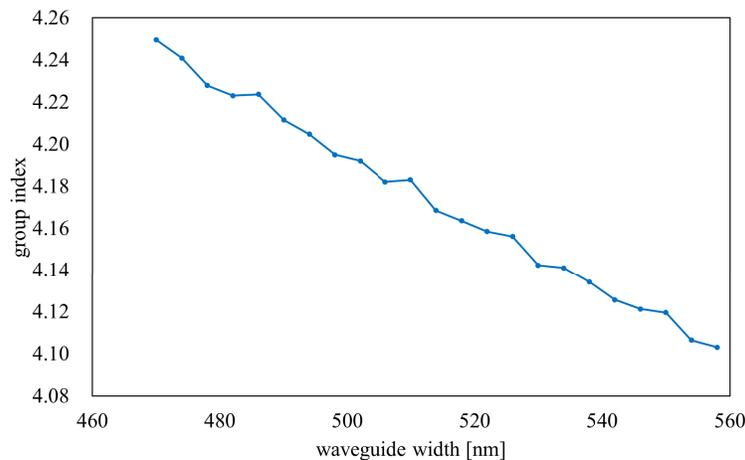
Fig. 5. Group index of waveguide with different width calculated from the simulated effective index in COMSOL Multiphysics.

range of 1545 nm to 1555 nm. Subsequently, the n_g at 1550 nm is calculated after fitting the n_{eff} over wavelength. In COMSOL Multiphysics, the refractive index of silicon is derived from Li [8].

We present the calculated n_g of waveguides with a fixed $t = 212$ nm but different width in Fig. 5.

Our findings demonstrate that the n_g values derived from the COMSOL simulation of n_{eff} do not present a consistent trend relative to the waveguide width, even though we employed the highest level of sampling resolution. Therefore, we did not use the COMSOL simulation results to establish the mapping database.

4. New mapping algorithm and MZI design

Earlier, we mentioned that significant changes in n_{eff} require the use of circuits with shorter delay lengths for parameter extraction. The fabrication deviation in waveguide width contributes 88% to the uncertainty of n_{eff}. To address this challenge, we used n_g to make a preliminary estimate of the fabricated waveguide width.

4.1. Ratio of the sensitivity of waveguide group index to thickness and width

We initiated an evaluation of the feasibility of determining the waveguide width utilizing solely the n_g. Initially, we assume that the waveguide thickness is a predetermined value, using only the n_g corresponding to the waveguide with the assumed thickness to calculate the width. Consequently, the variation in width, denoted as Δw, can be expressed as follows:

$$\Delta w = -Rng \times \Delta t = -\frac{\partial n_g}{\partial t} : \frac{\partial n_g}{\partial w} \times \Delta t. \tag{10}$$

The factor $Rng = \frac{\partial n_g}{\partial t} : \frac{\partial n_g}{\partial w}$ quantifies the extent of uncertainty associated with the initially calculated width. In the subsequent analysis, we will examine this parameter across the C-band and O-band, and both for Air-clad and SiO$_2$-clad waveguides.

In Fig. 6, we present the relationship between the factor Rng and waveguide width for waveguides with a constant thickness of 212 nm. It is evident that the group index n_g of the O-band oxide-clad waveguide and the C-band air-clad waveguide is largely invariant to variations in waveguide thickness. This indicates that the waveguide width can be determined with high precision using only the group index for these specific waveguides. The focus of this article is on the C-band oxide-clad waveguide, which exhibits relatively suboptimal performance. Nevertheless, it is noteworthy that the variation in width, denoted as Δw, can be minimized to approximately the same order of magnitude as the thickness differential, with $\Delta w \approx 0.9\, dt$ observed within the width range of 480 nm to 580 nm.

4.2. Fast-converging iterative mapping algorithm

We have demonstrated that for a C-band oxide-clad waveguide the uncertainty of waveguide width when calculating width based solely on n_g, is approximately 3 nm. This finding significantly reduces the contributions of dw to the dn_{eff}. Subsequently, the calculation of the waveguide thickness is conducted exclusively using n_{eff}, while assuming the previously determined waveguide width. Notably, the n_{eff} exhibits greater sensitivity to variations in thickness compared to width (as indicated in Eqs. (1) and (2)). This method further minimizes the error propagated from the calculated width to the calculated thickness.

As a result, a cyclic convergence algorithm has been developed. In the relationship $w = f(n_g, t)$, the calculated width has lower uncertainty than the input thickness. Meanwhile, in the relationship $t = g(n_{eff}, w)$, the calculated thickness also has lower uncertainty than the input width.

This algorithm requires the processing of only one variable at each iteration, thereby significantly simplifying computational complexity. In the subsequent sections, we will illustrate the mapping
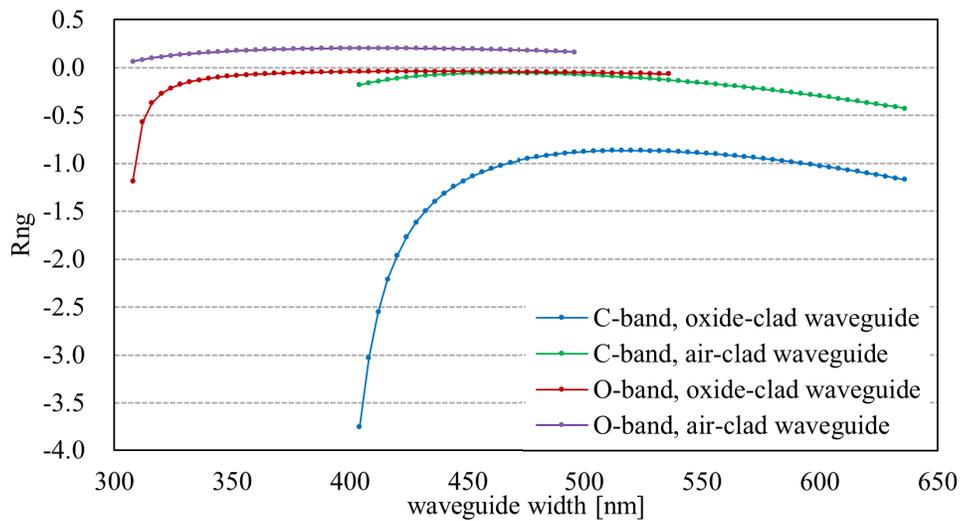
Fig. 6. Rng of waveguide with different width and a fixed thickness of 212 nm

errors and provide insights into designing the minimum length difference of the MZI, in conjunction with the application of this approach.

4.3. Mapping error

To evaluate the mapping error, we conducted simulations of the n_{eff} and the n_g of waveguides with widths ranging from 470 nm to 558 nm, incremented by 4 nm, and thicknesses spanning from 200 nm to 220 nm, also with a step size of 4 nm. The simulated values of n_{eff} and n_g were subsequently utilized to derive the waveguide dimensions. The mapping error is defined as the discrepancy between the original dimensions and the calculated dimensions. The mapping error for a waveguide with a thickness of 212 nm is presented in Fig. 7, illustrating the mapping error for waveguides of varying widths.
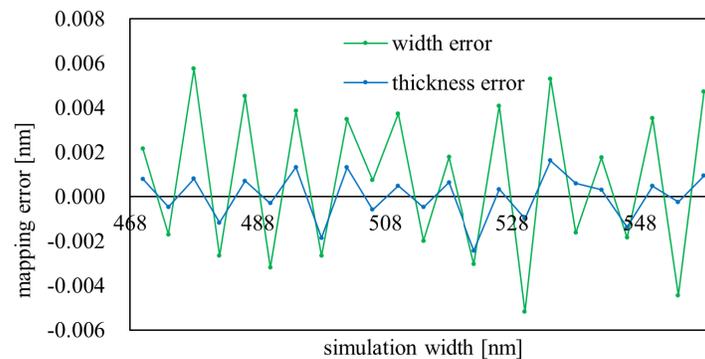
Fig. 7. Mapping error of the iterative algorithm.

As demonstrated in [7], the traditional mapping method exhibits significant error margins. Specifically, utilizing a third-order polynomial for fitting results in errors of $\Delta w_{mapping} = 0.06$ nm and $\Delta t_{mapping} = 0.08$ nm. In contrast, the implementation of the new mapping method reduces the error to $\Delta w_{mapping} = 0.006$ nm and $\Delta t_{mapping} = 0.002$ nm.

4.4.   MZI designed for the parameter extraction

For both C-band and O-band, encompassing both air-clad and oxide-clad waveguides, we assume a fabrication deviation of the waveguide parameters as $dw = 35$ nm and $dt = 3$ nm. In Table 1 we illustrate the minimal delay length required for the MZI to be utilized in our analysis.

Table 1. Minimal delay length of MZI to extract effective index

	expected t [nm]	designed w [nm]	minimal ΔL [μm]
O-band, air-clad	211.5	420	101.80
O-band, oxide-clad	211.5	420	114.74
C-band, air-clad	211.5	540	113.66
C-band, oxide-clad	211.5	540	100.36

Table 1 indicates that a Mach-Zehnder Interferometer with a delay length of $100\,\mu m$ can effectively be employed to determine the effective index. This specific MZI configuration is sufficiently high-order to also facilitate the direct extraction of the group index. Therefore, it is feasible to obtain the waveguide parameters utilizing a single-stage passive circuit.

5.   Fabrication

In our design, we have implemented a folded MZI structure, as illustrated in Fig. 8, which integrates two DCs functioning as both a splitter and a combiner. The widths of both arms of the MZI are meticulously calibrated to range from 482 nm to 546 nm, with an increment of 4 nm between each step. The delay length for all MZIs is established at $100\,\mu m$. These MZIs are developed on the die fabricated through the IMEC multiproject wafer (MPW) service.
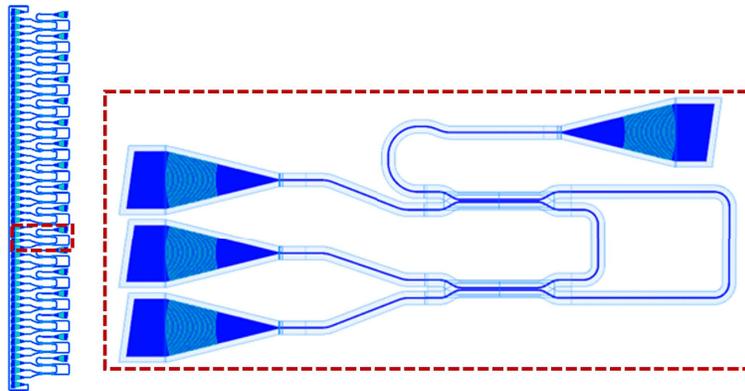
Fig. 8. Designed width sweep MZIs

It is worth mentioning that we do not use the extracted waveguide error to refer to the error of the waveguide on the entire die. If this method proves successful, we will make circuits for parameter extraction at different locations on the die in future designs to calculate the local variations at different locations on the die. We will then create die-level and wafer-level error trend graphs.

We employ parameter sweeps for two primary objectives:

1. The first objective is to validate the extraction process. By independently extracting n_{eff} from these MZIs, we anticipate obtaining a curve that effectively correlates n_{eff} with the designed waveguide width. The presence of jumps or discontinuities in the curve, or any

distortions when compared to the theoretical model, may indicate an erroneous extraction associated with the wrong interference order.

2. The second objective is to assess whether the deviations in the extracted dimensions correspond to the designed width values. For example, we seek to determine if a narrower waveguide leads to a more pronounced deviation in width.

6. Data analysis

We conducted measurements of the bar port transmission spectrum for all devices across eight distinct dies within the waveguide wavelength range of 1529.30 nm to 1571.27 nm, utilizing a step size of 0.001 28 nm, facilitated by the Luna Optical Vector Analyzer (LUNA OVA). During the measurement, there is no electrical signal input to the chip, and we use a temperature controller to keep the chip at approximately 20°C, which is consistent with the 293K used in the simulation database.

Figure 9 shows the measurement setup, which includes the LUNA OVA (top left), Polatis Switch (bottom left), Hexapod alignment system, and fiber array (right). The LUNA system outputs the measurement laser, which is connected to one of the 64 ports of the Polatis Switch via an optical fiber. The remaining ports of the Polatis Switch are directly connected to the fiber array. Using custom code, we control in real time which Polatis Switch port the measurement laser is routed to, enabling fully automated measurements of different circuits on a single die.
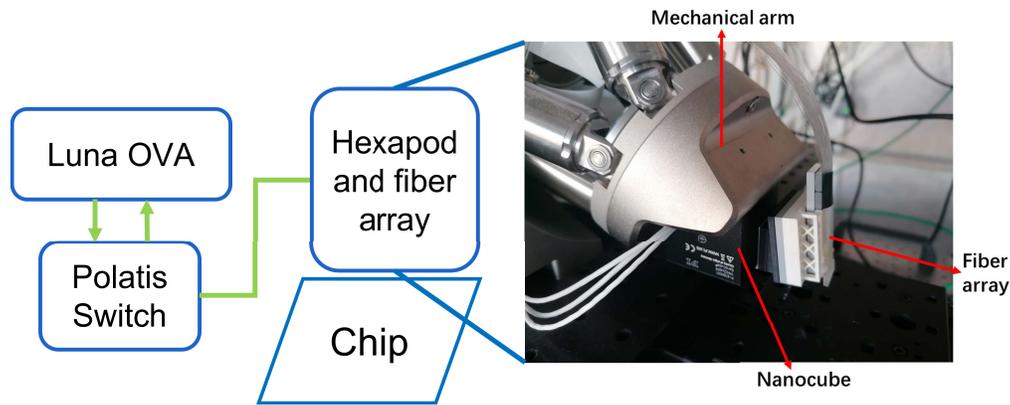
Fig. 9. Equipments used for the measurement

A representative measurement of the fiber-to-fiber transmission data for one bar port is presented in Fig. 10, where the blue line denotes the original measurement value, while the red line illustrates the signal subsequent to the application of a low-pass filter. We employ low-pass filters to remove reflections from the interface in the optical path, such as those from optical fibers and gratings. These reflection loops typically exceed the optical path length of the MZI, resulting in high-frequency oscillations in the measured spectrum. The green line represents the upper envelope of the signal, which has been calculated to eliminate the effects of fiber-to-chip coupling. The right image provides a detailed view of the original signal, focusing on the wavelength range between 1549 nm and 1551 nm (see the black rectangle in the left picture). The normalized measurement results are depicted in Fig. 11. This serves as the objective function that the mathematical model of the MZI requires for fitting.

Subsequently, this section will elucidate the rationale for selecting the bar port measurement results for data processing rather than the cross port.
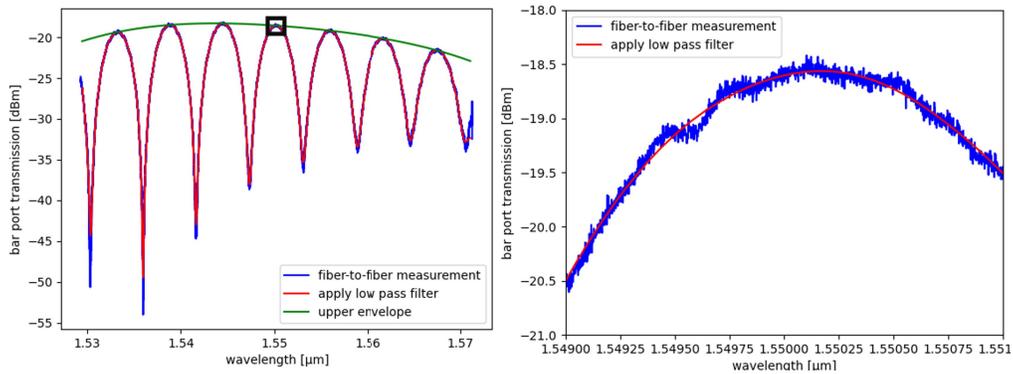
Fig. 10. Bar port transmission spectrum of one of the designed MZIs

6.1.　Simulation of a dispersive MZI

We conducted a simulation of the transmission spectrum of an MZI, with the results presented in Fig. 12. In this MZI, both the waveguide and DC models exhibit dispersive characteristics, with the DC demonstrating a 50/50 coupling ratio at a wavelength of 1550 nm.

The upper envelope of the transmission spectrum for the MZI bar port, in the absence of a grating, is theoretically expected to achieve a value of 1, provided that the two directional couplers within the MZI possess identical coupling rates. This characteristic can be leveraged to effectively eliminate fiber-to-chip coupling effects. Conversely, the upper envelope of the cross port will be influenced by the coupling ratios of the directional couplers within the MZI, making it unsuitable for data normalization purposes.

Nevertheless, evaluating the bar port measurement spectrum does not readily indicate whether the two directional couplers are equivalent. In this context, it becomes essential to examine the lower envelope of the cross port: the theoretical expectation for the lower envelope of the
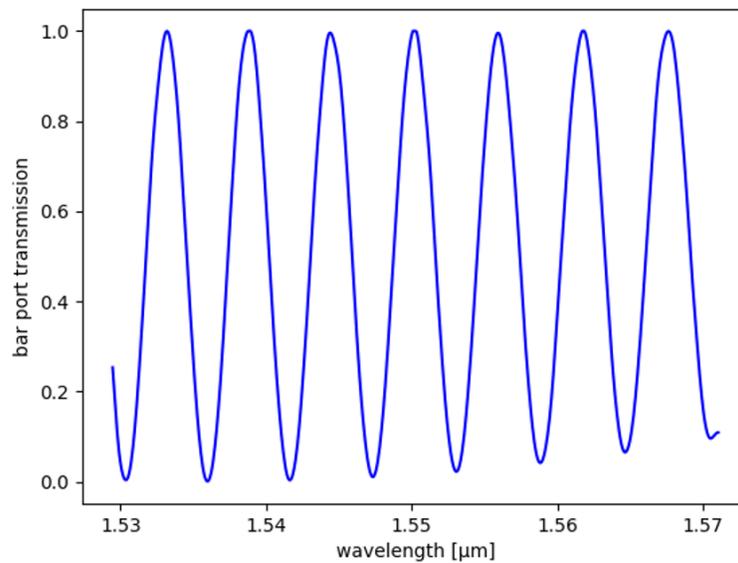
Fig. 11. Normalized spectrum of one of the MZIs
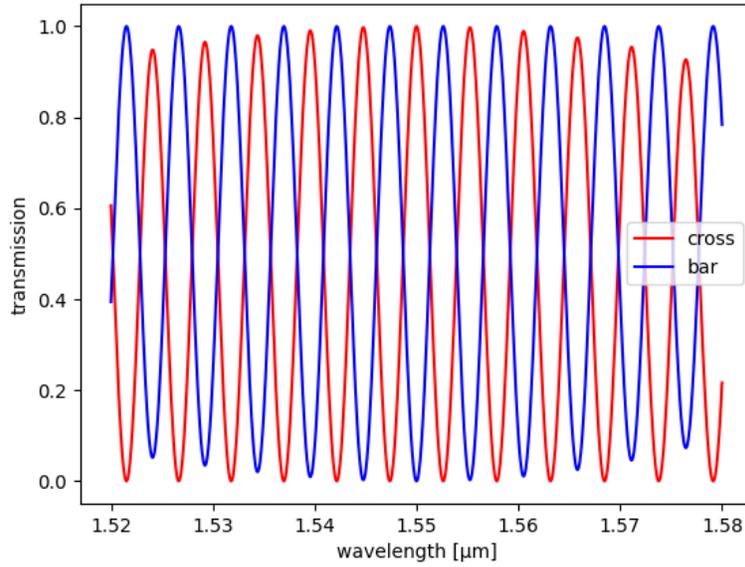
Fig. 12. Simulation results of MZI bar and cross ports' transmission spectrum

cross port is 0, which corresponds to negative infinity on a dB scale. Any deviation from this would indicate a discrepancy in the coupling ratios of the two directional couplers. In practical measurements, however, even when the coupling coefficient of the two DCs in a MZI is identical, various factors can influence the lower envelope of the spectrum at the cross port, including the scanning step length of the light source and the background noise present in the measurement optical path. As a result, achieving a lower envelope value of zero in the measurement is unfeasible.

In terms of light source scanning wavelength step we utilized wavelength data from the light source that aligns with the actual measurements in the simulation of the MZI. Our findings indicate that, with a light source exhibiting a step length of 0.001 28 nm, the cross-port spectrum lower envelope of the MZI is approximately −70 dBm.

The zero input feedback of the Luna OVA registers around −50 dBm to −60 dBm. In analyzing the actual measurement data, the envelope value of the cross port spectrum typically ranges from −60 dBm to −65 dBm. This range is lower than the background noise level observed in the absence of any signal. This phenomenon can be attributed to the filtering techniques employed by the Luna OVA device, which effectively minimize measurement noise.

We assert that when the lower envelope of the cross-port spectrum is larger than −60 dBm, it indicates a disparity in the coupling coefficients of the two DCs within the MZI. This discrepancy may introduce unknown additional phases, thereby impacting the integrity of the measurements. Consequently, such data will be disregarded in our analysis.

6.2. Extract waveguide n_{eff} and n_g

In this section, we will detail the methodology employed to extract the n_{eff} and n_g of the waveguide within the designed MZI. A second-order dispersion model for n_{eff} is utilized, as delineated in Eq. (11):

$$n_{eff}(\lambda) = n_{eff}(\lambda_0) + (\lambda - \lambda_0) \times \frac{\partial n_{eff}}{\partial \lambda} + \frac{1}{2}(\lambda - \lambda_0)^2 \times \frac{\partial^2 n_{eff}}{\partial \lambda^2} \qquad (11)$$

where λ_0 is defined as 1550 nm. The group index n_g is subsequently determined using the following formula:

$$n_g(\lambda) = n_{eff}(\lambda) - \lambda \frac{\partial n_{eff}(\lambda)}{\partial \lambda}. \tag{12}$$

During the fitting process, n_{eff} and n_g are used to calculate the phase difference between the two arms of the MZI, as described by Eq. (13):

$$M_{arm} = \begin{bmatrix} \exp -\frac{i2\pi n_{eff}(\lambda)\Delta L}{\lambda} & 0 \\ 0 & 1 \end{bmatrix}. \tag{13}$$

Where ΔL represents the length difference between the two arms of the MZI.

We first extract the approximate n_g from the spectrum and then estimate the waveguide width assuming a thickness of 212 nm. Using this width and thickness, we calculate an initial value for n_{eff} to guide the fitting. The fitting range for n_{eff} is constrained to prevent the occurrence of two optimal values, ensuring a unique solution. Finally, we calculate n_g using Eqs. (11) and (12). Through this methodology, we extract the n_{eff} and n_g from the spectra of each circuit. The results are depicted in Fig. 13, which illustrates that n_{eff} increases with the designed waveguide width, whereas n_g exhibits a decreasing trend as the designed width expands.
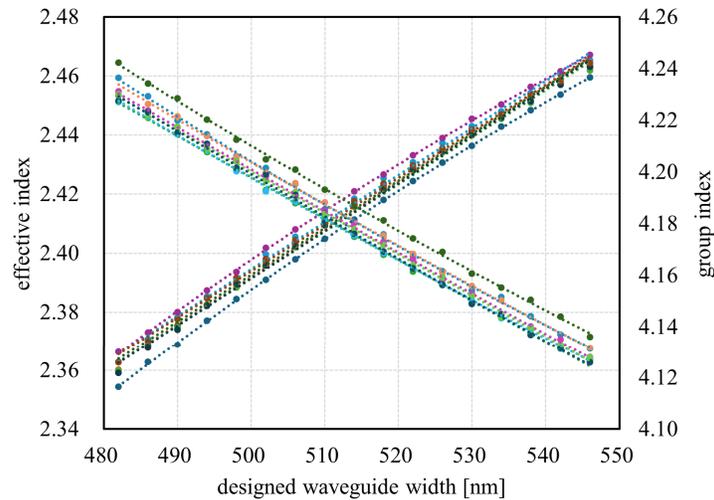
Fig. 13. Extracted effective and group index of the arm waveguides in all circuits

The n_{eff} of the waveguide in each sample demonstrates a continuous and smooth variation in response to the designed width. This observation indicates that there is no confusion regarding the interference order in some of the circuits during the parameter extraction process. However, Fig. 13 does not provide clarity on whether all spectral interference orders may be shifted together (for instance, whether all extracted interference is uniformly shifted by +1 or −1) throughout the parameter extraction process. We will return to this question after extracting the waveguide thickness.

6.3. Extraction of waveguide width and thickness

In this section, we present the waveguide geometric parameters obtained through the mapping algorithm, utilizing the extracted values of n_{eff} and n_g. It is noteworthy that the deviations in width, denoted as δw (where δw represents the difference between the extracted value and the designed value), are illustrated in Fig. 14 rather than the widths themselves.
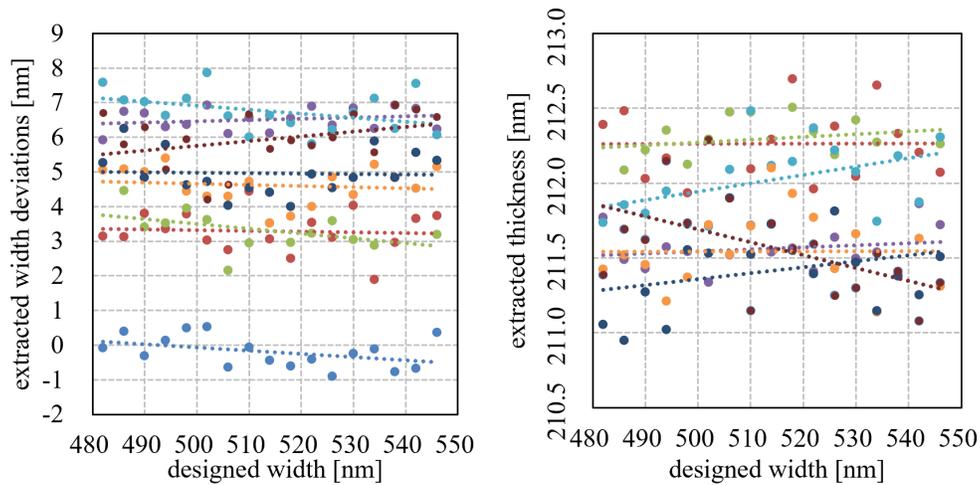
Fig. 14. Extracted waveguide width deviations (left) and thickness (right) of the arm waveguides in the designed MZIs.

The maximal value of δw are 7.87 nm and the maximal value of extracted thickness are 212.70 nm, whereas the minimal values are recorded as -0.90 nm and 210.95 nm, respectively. We calculate the maximum fabrication deviation of waveguide width to be 8.77 nm, which is notably smaller than the previously reported measurement value of 35 nm. We attribute this discrepancy to the earlier measurements being derived from more dies, particularly those at the wafer's edge, which may exhibit larger manufacturing deviations. The mean thickness extracted is 211.77 nm, while the mean width deviation is 4.42 nm.

The designed arm length difference in the MZI allows for the extraction of thickness variations of up to 3 nm without inducing confusion in the interference order. Measurement results across various dies indicate that all extracted thicknesses cluster around the mean value, with a maximum deviation of less than 2 nm. When considering the possibility of confusion among diffraction orders in the spectrum, the extracted average waveguide thickness may be expressed as 211.77 nm $\pm$ 3 nm $\times m$, where m is an integer. The average thickness measured via ellipsometry is 212 nm, with a maximum deviation of 3 nm observed across different dies. The mean waveguide thickness obtained from parameter extraction closely aligns with the mean thickness derived from measurement. Therefore, we verified by extracting the waveguide thickness that the measurement interference order has not shifted compared with the original design.

The variations in waveguide width errors and waveguide thickness exhibit a notable degree of independence across different values of designed waveguide width. This observation may suggest that, within the examined range and under current processing conditions, the fabrication deviations in waveguide width are not correlated to the designed widths.

6.4. Comparison of results with others

In [4], the authors designed a waveguide with an initial thickness of 220 nm and a width of 450 nm. After fabrication on the IMEC 200 mm CMOS pilot line, their extraction results indicated a waveguide width of 470 nm $\pm$ 4 nm and a thickness of 211 nm $\pm$ 1 nm.

The same waveguide design was implemented in [7], where fabrication was also carried out using IMEC's multiproject wafer services. The extracted waveguide width for dies near the wafer center ranged from 468.8 nm to 471.9 nm, while the thickness ranged from 211.4 nm to 212.3 nm. The extracted waveguide width on the die near the boundary of the wafer ranges from 461.4 nm to 466.8 nm, and the thickness ranges from 212.1 nm nm to 214.0 nm.

The waveguide thickness extraction results in this work are consistent with those reported for waveguides fabricated using similar processes. The average values and deviation ranges of the waveguide thickness we extracted are very close.

The average waveguide width manufacturing error extracted from our experimental measurements is 4.42 nm, which is significantly smaller than previously reported values (ranging from 11 nm to 20 nm). The maximum width error range is relatively close, approximately 8 nm to 10 nm. This is because in recent years, IMEC has changed the width compensation applied during manufacturing, which has reduced the width deviation of +20 nm to a deviation of a few nanometers. However, the manufacturing process has not been innovated, so the width deviation range has not changed significantly.

7. Estimation of extraction error and discussion

In this above, we outline the various steps undertaken throughout the parameter extraction process. We proceed to calculate the error associated with each step in the extraction procedure.

7.1. Errors arising from simulations of waveguide n_{eff} and n_g

As discussed in Section 3.2, the refractive indices reported in different databases exhibit variability, which can lead to differing results in parameter extraction. The true refractive index of the material remains unknown; hence, we compare results derived from the databases of Li and Franta.

The discrepancy in the material refractive index between the two databases is found to be 0.0036, while the difference noted in their dispersion is $0.006\,\mu m^{-1}$. The n_{eff} of a waveguide with a width of 510 nm and a thickness of 212 nm, calculated using Li's database, is lower than that calculated with Franta's database by 0.003. In contrast, n_g is lower by $0.01\,\mu m^{-1}$. These results indicate that utilizing Li's data as the mapping database results in an extracted waveguide width that is approximately 4 nm narrower and a thickness that is about 2.4 nm thicker compared to using Franta's data.

The accuracy of each database remains uncertain, and it is possible that both may not be precise. This type of error influences the absolute dimensions extracted; however, it does not significantly affect the relative deviations observed across different circuits and locations on the wafer.

7.2. Normalization and fitting errors

The methodologies applied for filtering fiber-chip coupling in the measurement data and for removing high-frequency oscillations associated with Fabry-Pérot reflections in the optical path also play a significant role in the extraction process. We executed the parameter extraction utilizing a specific dataset on 100 separate occasions, introducing random noise uniformly distributed within the range of ±0.2dBm to the measurement values at each wavelength point. The deviations observed in the results of these parameter extractions encompass errors from the removal of the grating envelope as well as fitting errors.

Our findings indicate that the standard deviations of the extracted n_{eff} and n_g are 1.46×10^{-6} and 1.59×10^{-4}, respectively. Regarding the extracted width and thickness, the standard deviations are 0.058 nm and 0.030 nm, respectively. Errors were estimated at three times the standard deviations, resulting in a confidence interval of 99.7%. Consequently, the errors attributable to data normalization and fitting are estimated to be 0.173 nm for width and 0.090 nm for thickness, maintaining a 99.7% confidence interval.

This type of error should be categorized as random error, directly impacting the relative extraction parameters among different devices.

7.3. Deviations in waveguide side wall angles

Initially, it was assumed that the angle of the waveguide side wall (base angle) α was 85°. In this section, we will analyze the errors induced by deviations in α ($\Delta\alpha$). For the purpose of this analysis, we will assume that $\Delta\alpha = 1°$.

We adjusted the waveguide side wall angle to 86° and established the corresponding mapping database. Utilizing this mapping, we extracted the waveguide width and thickness. The results indicate that an increase of $+1°$ in the base angle corresponds to a decrease of -3.610 nm in the width and a decrease of -0.037 nm in the thickness of the extracted geometry. The extraction error resulting from $\Delta\alpha$ should also be considered as a random error, which influences the relative extracted width and thickness across different circuits.

7.4. Total error

We cannot accurately calculate the total extraction errors, but we only consider the quantifiable factors and give the error reference as follows:

$$w_{Li} - w_{\text{Franta}} \approx -4.0 \text{ nm}$$

$$t_{Li} - t_{\text{Franta}} \approx 2.4 \text{ nm}$$

$$\Delta w_{\text{normalization+fitting}} (3\sigma) = 0.173 \text{ nm}$$

$$\Delta t_{\text{normalization+fitting}} (3\sigma) = 0.090 \text{ nm}$$

$$\Delta w_{\Delta\alpha=1°} = 3.61 \text{ nm}$$

$$\Delta t_{\Delta\alpha=1°} = 0.037 \text{ nm}$$

$$\Delta w_{\text{mapping}} < 0.006 \text{ nm}$$

$$\Delta t_{\text{mapping}} < 0.002 \text{ nm}.$$

For the random error, we believe it should be the sum of the three random errors mentioned above, which can be given by:

$$\Delta w_{\text{random}} = \pm 1.89 \text{ nm}$$

$$\Delta t_{\text{random}} = \pm 0.06 \text{ nm}.$$

7.5. Discussions

The primary limitation of our approach lies in the restricted range of waveguide thickness variation that is permissible. For instance, an arm length difference (ΔL) of 100 μm can facilitate the extraction of waveguide parameters when the maximum allowable thickness deviation is 3 nm. Conversely, if the waveguide thickness varies by ± 5 nm, the maximum ΔL achievable reduces to 29 μm. This limitation is significant and underscores the need to develop more efficient components for parameter extraction, without necessitating an increase in circuit size or data processing complexity.

Despite the advancements made by our new mapping algorithm in minimizing mapping errors, a considerable proportion of parameter extraction errors can be attributed to uncertainties in the material refractive index database and deviations in the side wall angle. Our algorithm does not significantly contribute to enhancing the overall absolute extraction accuracy (systematic error), given that both width and thickness extraction inaccuracies may exceed 1 nm due to simulation database limitations. Furthermore, it is observed that 95% of the random error in width can be ascribed to $\Delta\alpha$ (assuming $\Delta\alpha = 1°$), indicating that our method has minimal impact on reducing random width errors. Nevertheless, our new mapping algorithm proves beneficial in diminishing the relative error associated with the extracted thickness.

Our calculations indicate that the random extraction error for thickness remains within 0.12 nm, and our method effectively mitigates this type of error.

8. Conclusions

In this study, we have presented a mapping algorithm that operates in conjunction with a high-order MZI to derive actual waveguide parameters, including width, thickness, effective index and group index. The implementation of a fast-converging iterative algorithm allows for parameter extraction using a 100 μm delay-length MZI from the bar port transmission spectrum, without ambiguity regarding interference order. This advancement not only enhances extraction accuracy but also enables the acquisition of high-precision parameters through a single compact device, requiring only a single measurement and simplified data processing. The waveguide parameters we obtained from multiple samples closely align with those derived from our previous measurements, suggesting that this compact design, coupled with the iterative algorithm, will be highly beneficial for process monitoring.

We have critically analyzed sources of parameter extraction error that have previously been overlooked. It is evident that the absolute extraction error concerning waveguide dimensions predominantly arises from uncertainties related to the material refractive index across various databases. Additionally, we find that 95% of the relative error in extracted width can be attributed to uncertainties in the side wall angle (assuming $\Delta\alpha = 1°$). At present, we maintain that these two significant factors cannot be effectively mitigated through the design of more sophisticated circuits or enhanced parameter extraction algorithms. If there are no disclosures, then list "The authors declare no conflicts of interest."

Disclosures. The authors declare that there are no conflicts of interest related to this article.

Data availability. Data underlying the results presented in this paper are not publicly available at this time but may be obtained from the authors upon reasonable request.

References

1. L. Chrostowski and M. Hochberg, *Silicon Photonics Design: From Devices to Systems* (Cambridge University Press, 2015).
2. M. Milosevic, S. Stankovic, S. Reynolds, *et al.*, "The emergence of silicon photonics as a flexible technology platform," Proc. IEEE **106**(12), 2101–2116 (2018).
3. Y. Xing, J. Dong, M. U. Khan, *et al.*, "Capturing the effects of spatial process variations in silicon photonic circuits," ACS Photonics (2022).
4. S. Dwivedi, T. V. Vaerenbergh, A. Ruocco, *et al.*, "Measurements of effective refractive index of soi waveguides using interferometers," in *Advanced Photonics 2015*, (Optica Publishing Group, 2015), p. IM2A.6.
5. E. Zhang, X. Zhu, and L. Zhang, "Effective and group refractive index extraction and cross-sectional dimension estimation for silicon-on-insulator rib waveguides," Opt. Express **32**(18), 31375–31388 (2024).
6. Y. Xing, M. Wang, A. Ruocco, *et al.*, "Compact silicon photonics circuit to extract multiple parameters for process control monitoring," OSA Continuum **3**(2), 379–390 (2020).
7. Y. Xing, J. Dong, S. Dwivedi, *et al.*, "Accurate extraction of fabricated geometry using optical measurement," Photonics Res. **6**(11), 1008–1020 (2018).
8. H. H. Li, "Refractive index of silicon and germanium and its wavelength and temperature derivatives," J. Phys. Chem. Ref. Data **9**(3), 561–658 (1980).
9. D. Franta, A. Dubroka, C. Wang, *et al.*, "Temperature-dependent dispersion model of float zone crystalline silicon," Appl. Surf. Sci. **421**, 405–419 (2017). 7th International Conference on Spectroscopic Ellipsometry.
10. E. D. Palik, *Handbook of optical constants of solids*, vol. 3 (Academic press, 1998).